

Evidence that global processing does not limit thresholds for RF shape discrimination

Kathy T. Mullen

McGill Vision Research, Department of Ophthalmology,
McGill University, Montréal, Canada



William H. A. Beaudot

McGill Vision Research, Department of Ophthalmology,
McGill University, Montréal, Canada



Iliya V. Ivanov

McGill Vision Research, Department of Ophthalmology,
McGill University, Montréal, Canada



In studies of shape processing, a crucial distinction is made between the global stages, which integrate across features to define shape, and earlier stages that encode individual components. We investigate whether shape discrimination thresholds for radial frequency (RF) patterns are limited at this global stage or whether the information in individual components supports threshold. We use achromatic and chromatic (L/M- and S-cone opponent) radial frequency (RF) patterns of different contour thicknesses (0.75–6 cpd). First, we show using sections of an RF4 that shape discrimination thresholds are invariant with cycle number from 1 to the complete pattern. Performance for a single cycle displayed alone is as good as for the whole RF, indicating that information within a single RF cycle is sufficient to support the whole shape discrimination threshold, arguing against an influence of global processing. Second, we find similar thresholds for the discrimination of RF patterns and modulated line stimuli, also arguing against global effects. Third, we calculate a metric for the intrinsic orientation variation in a stimulus cycle at threshold and show that this potentially accounts for the improvement in shape and line discrimination thresholds with modulation frequency from RF1 to RF6. Higher threshold discrimination for chromatic compared to achromatic patterns may reflect the poorer orientation discrimination of color vision, rather than a deficit for global processing. We propose that the global stages of shape processing are not revealed at threshold but are enabled only for well-defined shapes at suprathreshold modulations.

Keywords: shape discrimination, spatial vision, color vision, radial frequency, isoluminance, orientation discrimination, global

Citation: Mullen, K. T., Beaudot, W. H. A., & Ivanov, I. V. (2011). Evidence that global processing does not limit thresholds for RF shape discrimination. *Journal of Vision*, 11(3):6, 1–21, <http://www.journalofvision.org/content/11/3/6>, doi:10.1167/11.3.6.

Introduction

Simple shape processing is hierarchical and involves multiple stages beginning with an initial stage of encoding local orientation information in the shape, followed by intermediate stages in which local curvature or angles are processed. In the next “global” stage, considered to be a key aspect of the hierarchy, these distributed features are integrated over space to extract an overall form, and by the highest stage, shape is encoded independently of spatial scale and retinal position (Bell, Badcock, Wilson, & Wilkinson, 2007; Hess, Wang, & Dakin, 1999; Levi & Klein, 2000; Loffler, Wilson, & Wilkinson, 2003; Webb, Roach, & Peirce, 2008; Wilkinson, Wilson, & Habak, 1998; Wilson, 1999; Wilson & Wilkinson, 1997). The physiological origins of these different shape processing stages are not yet well understood but begin in V1 and V2 with local orientation (Hubel & Wiesel, 1968) and curvature extraction (Dobbins, Zucker, & Cynader, 1987, 1989), progress through V4 with concentric and curvature-based

neural responses (Dumoulin & Hess, 2007; Gallant, Braun, & Van Essen, 1993; Gallant, Shoup, & Mazer, 2000; Pasupathy, 2006; Pasupathy & Connor, 1999; Wilkinson et al., 2000), and are thought to become invariant to position and spatial scale within the higher stages of the inferotemporal cortex (Webb et al., 2008).

An experimentally useful stimulus for the investigation of shape perception is the radial frequency (RF) pattern (Wilson & Wilkinson, 1997), which is a radially modulated contour (usually defined by a fourth derivative of a Gaussian) representing simple, concentric shapes such as ellipses, triangles, squares, etc. These patterns have been used psychophysically to investigate shape processing by measuring radial modulation thresholds for the discrimination of the radial frequency shape from a perfect circle (Bell et al., 2007; Hess et al., 1999; Jeffrey, Wang, & Birch, 2002; Loffler, 2008; Loffler et al., 2003; Mullen & Beaudot, 2002; Poirier & Wilson, 2007; Wang & Hess, 2005; Wilkinson et al., 1998; Wilson, 1999).

Psychophysical thresholds for shape discrimination may potentially be limited at any of the hierarchical processing

stages described above. It has been argued, however, that the threshold discrimination of radial frequency patterns is determined by the higher, global processing stage that integrates across stimulus cycles rather than the earlier stages that encode individual components of the pattern (Bell & Badcock, 2008; Hess et al., 1999; Loffler et al., 2003; Wilkinson et al., 1998). Various lines of evidence have been used to argue for this. One approach is to compare discrimination thresholds for a whole pattern with those for a local section of it, such as an individual feature (corner, side etc.), or a single cycle of radial frequency modulation. Hess et al. (1999) found that shape discrimination thresholds are better for an intact RF pattern than for a random rearrangement of its component parts. They reasoned that global processes determine shape discrimination thresholds because global, but not local, cues are disrupted by the rearrangement. Bell and Badcock (2008), Hess et al. (1999), and Loffler et al. (2003) measured discrimination thresholds for RF patterns as a function of the numbers of cycles of modulation displayed. These authors found an improvement in performance with increasing cycle number that was greater than that predicted from probability summation and concluded that the global pooling limits threshold for patterns of relatively low radial frequencies ($RF < 10$). In this paper, we return to the issue of how shape discrimination thresholds are limited. We use experiments designed to separate the contributions from the earlier local and intermediate processing stages, which encode individual components of the stimulus, from the global processing stages, which integrate these components into a whole, concentric shape.

A second approach to this issue relates to the form of the function describing shape discrimination thresholds versus radial frequency. This shows an initial improvement as radial frequency increases up to 4–6 cycles/pattern (Mullen & Beaudot, 2002; Wilkinson et al., 1998). This initial improvement in threshold with RF may indicate the use of localized orientation variation or curvature in the stimulus contour, since these stimulus cues also increase with radial frequency. To test this issue, Wilkinson et al. (1998) measured discrimination between a fixed RF pattern and circles of varying diameters and hence different curvatures, which were selected to span a wider curvature range than found in the RF pattern. As no disruption to threshold occurred, they argued that local curvature comparisons between the RF pattern and a circle were not the basis of shape discrimination thresholds and concluded that the threshold instead must be limited by a higher, global stage. Although these experiments may indicate that local curvature is irrelevant to threshold, alternatively, they may simply imply that the task of discrimination from circular can be performed without a direct comparison with a circle, something we explore in this paper.

Psychophysical evidence has shown that shape discrimination thresholds for RF patterns are significantly poorer for color than for luminance vision with both cone

opponent mechanisms (L/M and S) performing worse than the achromatic mechanism (Mullen & Beaudot, 2002). Although this deficit for color is not dramatic, it is consistent over a wide range of contrast values and radial frequencies. An important question arising is whether this effect reveals a deficit of global processing for color vision or whether, instead, it reflects impoverished orientation coding at the earlier local or intermediate stages in shape processing. Color vision is less sensitive to orientation differences than luminance vision (Beaudot & Mullen, 2005; Webster, De Valois, & Switkes, 1990), and a reliance on local orientation differences at shape discrimination threshold might account for the reduced performance of color compared to luminance vision. Thus, this difference in performance between color and luminance vision in shape discrimination may be better understood by elucidating the link between local and global cues at shape discrimination threshold.

We undertake a series of experiments with the aim of determining, for color and luminance vision, whether non-global cues, occurring prior to the integration across multiple stimulus cycles, limit threshold shape discrimination of radial frequency patterns. In our first approach, the crucial distinction we make is that the local and intermediate stages of shape processing use information contained within one stimulus cycle, whereas the global stages require integration across stimulus cycles to extract the overall shape. We compare the discrimination thresholds for single components of the stimuli to those for the radial frequency pattern as a whole. If a process of global integration limits thresholds, we should expect discrimination for the whole shape to be better than for its local components, taking the effects of probability summation into account. In a second set of experiments, we extend this argument by comparing discriminations for a circular and linear contour: the same contour is presented either as a modulated line, or closed to form the radial shape of the RF pattern. If global processing is limiting discrimination thresholds for the RF patterns, subjects should be better at detecting the contour in the form of a concentric shape than in the form of a modulated line (Hess et al., 1999; Wilkinson et al., 1998). In the third part of the paper, we calculate the orientation variation present within one cycle of the RF and line stimuli under different conditions of radial frequency, radius, and chromaticity in order to assess whether cues based on orientation discriminations could account for the threshold performance for simple shapes (radial frequencies up to 6). We further distinguish between local stimulus cues that are intrinsic to the contour or depend on direct comparisons with the perfect circle (extrinsic to the contour). Our overall results support the idea that non-global cues, based on intrinsic orientation discriminations within one stimulus cycle, limit the threshold discrimination of simple shapes. This concurs with recent proposals (Bell, Gheorghiu, & Kingdom, 2009; Bell & Kingdom, 2009; Bell, Hancock, Kingdom, & Peirce,

2010) that tasks relying on judgments of the suprathreshold appearance of shapes may be better at revealing global processing than threshold-based tasks.

Methods

Stimuli

The stimuli used were chromatic, isolating the L/M- and S-cone opponent mechanisms, and achromatic radial frequency patterns, or modified versions of these stimuli. The radial frequency patterns were radially modulated D4s (fourth derivative of a Gaussian; Wilkinson et al., 1998; Wilson & Wilkinson, 1997), with peak spatial frequencies of 0.75–6 cpd, whose contrasts were equated in multiples of detection threshold. Comparisons between chromatic and achromatic stimuli were made only for stimuli of 0.75 and 1.5 cpd in order to minimize the effects of chromatic aberrations in the color stimuli (Bradley, Zang, & Thibos, 1992) and to ensure effective isolation of chromatic mechanisms. These radial frequency patterns are band-limited in spatial frequency domain and defined by the following equations:

$$RF(r) = L_m \left[1 + c(1 - 4r^2 + 4r^4/3)e^{-r^2} \right], \quad (1)$$

$$r(x, y) = \frac{\sqrt{x^2 + y^2} - R(x, y)}{\sigma}, \quad (2)$$

$$R(x, y) = R_m \{ 1 + A \sin[f_r \arctan(y/x) + \theta] \}, \quad (3)$$

$$\sigma = \frac{\sqrt{2}}{\pi \omega_p}, \quad (4)$$

where σ is the space constant of $RF(r)$ in degrees, and ω_p is the D4 peak spatial frequency. $R(x, y)$ is the sinusoidal radial modulation of D4s, where R_m is the mean radius (2.4 deg, unless otherwise stated), f_r is the radial frequency, A is the amplitude of the radial modulation, and θ is the phase of the modulation (randomly selected in each trial of the experiments). L_m and c are the mean luminance and contrast, respectively. Circular patterns have no radial modulation ($A = 0$, and thus R is constant). The subject's task was to discriminate between a non-modulated (perfectly circular) and a radially modulated stimulus.

In Experiment 1, we use subsections of the radial frequency pattern generated by suppressing the contrast around most of the radial contour with a Gaussian contrast envelope, defined by the following equations:

$$C(x, y) = C_m \left[1 - e^{-(\arctan(y/x) - \theta_c)^2 / (2\sigma_c^2)} \right], \quad (5)$$

$$RF_C(r) = L_m \left\{ 1 + c[1 - 4r^2 + 4r^4/3]e^{-r^2} \cdot [1 - C(r)] \right\}, \quad (6)$$

where $C(x, y)$ is the Gaussian radial contrast modulation of D4s centered on θ_c . σ_c is the angular space constant, C_m is the factor of contrast attenuation (1), and θ_c is the phase of the contrast modulation relative to the phase of the radial modulation (0 deg for sides only or 180 deg for corners only). σ_c was set to 30 degrees in order to display a single cycle centered on either a convex (“corner”) or concave (“side”) piece of the radial frequency pattern, depending on the location of the peak of the Gaussian envelope. A sigma of 30 deg was the minimum sigma required to display a full stimulus cycle (spanning 90 deg in RF4) centered on either corners or sides. All other stimulus parameters were the same as for the whole pattern, including the random selection of the phase of the radial pattern, which varied the angular location of the selected feature. Examples are shown in the icons in Figure 1.

In Experiment 2, we measure modulation thresholds for a line stimulus. The line stimulus (illustrated by the icons in Figure 4) is made of the same D4 contour as the radial pattern but is linearly rather than radially modulated. The equations for the line are the same as for the circular pattern, except for Equation 3 that is replaced by

$$R(x, y) = R_m \cdot A \cdot \sin[f_r \cdot y + \theta]. \quad (7)$$

Chromatic representation of the stimuli

Stimuli were represented in a three-dimensional cone-contrast space (Cole, Hine, & McIlhagga, 1993; Eskew, McLellan, & Giulianini, 1999; Sankeralli & Mullen, 1996, 1997) in which each axis is defined by the incremental stimulus intensity for each cone type to a given stimulus normalized by the respective intensity of the fixed adapting white background. Cone excitations for the L-, M-, and S-cones were calculated using the cone fundamentals of Smith and Pokorny (1975). A linear transform was calculated to specify the required phosphor contrasts of the monitor for given cone contrasts. Post-receptoral luminance, L/M-cone opponent, and S-cone opponent mechanisms were modeled as linear combination of cone-contrast responses and were isolated by using the achromatic (L + M + S), red–green (L – α M), and blue–yellow (S-cone)

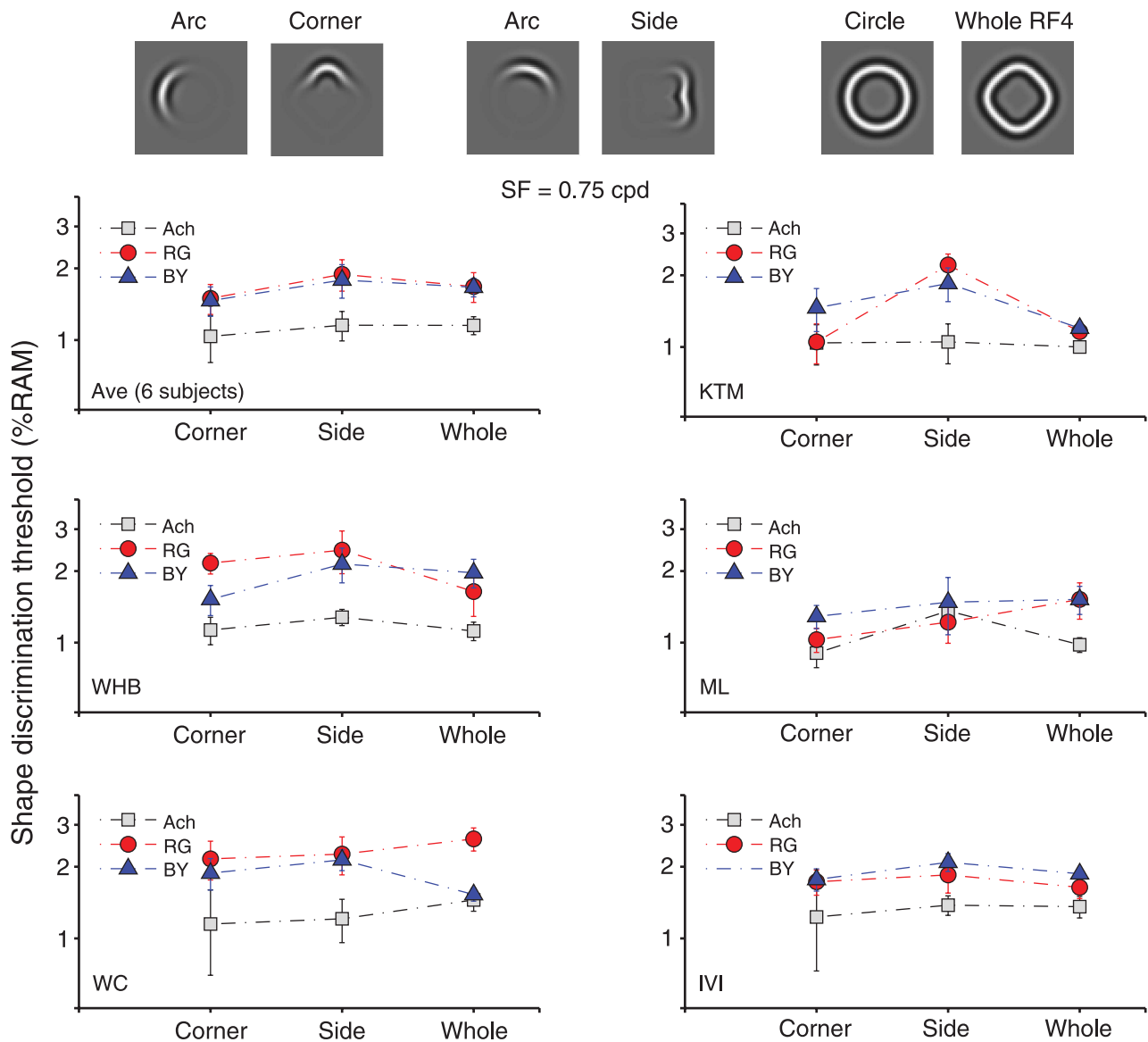


Figure 1. Shape discrimination thresholds (% radial amplitude modulation) are plotted for three different conditions as illustrated in the icon pairs: a full radial frequency pattern (RF4, top right pair), a section of the full pattern representing a "side" part (middle pair), and a section representing a "corner" (left pair). In each case, discrimination is between the RF pattern (0.75 cpd, radius = 2.4 degrees) and the equivalent part of the perfect circle. Phase is varied between individual stimulus presentations. Different symbols represent results for red–green (RG), blue–yellow (BY), and achromatic (Ach) stimuli. Different panels show results for 5 of 6 subjects, and the top left panel shows the average of all 6 subjects. Contrast is set to 5× contrast detection threshold for each of the test stimuli (corner, side, and whole) except for subjects IVI (lower right panel) and LA (not shown), who were run as a control with the contrast of all stimuli set to 5× detection threshold for the whole pattern. We also verified in three of our subjects that these results are unchanged at higher suprathreshold contrasts of 10 and 20 times threshold (data not shown). Error bars show ±1 SE. Average stimulus cone contrasts were: Ach, 3.35% (whole RF), 8.2% (corner/side); RG, 1.04% (whole RF), 2.6% (corner/side); BY, 6.72% (whole RF), 13.2% (corner/side). For IVI: 3% for Ach, 0.8% for RG, and 5% for BY.

cardinal stimuli, where α is a numerical constant obtained at isoluminance. Stimulus contrast is defined as the root mean square or the vector length in cone-contrast units (C_C):

$$C_C = \sqrt{(L_C)^2 + (M_C)^2 + (S_C)^2}, \quad (8)$$

where L_C , M_C , and S_C represent the L, M, and S Weber cone-contrast fractions in relation to the L-, M-, and S-cone values of the achromatic background. The inter-subject variability found for the luminance mechanism affects the specification of the red–green (isoluminant) cardinal direction. For each observer and for each spatial frequency, the isolation of the red–green mechanism at

isoluminance (value of α above) was estimated by a minimum motion task in the cone-contrast space (Cavanagh, Tyler, & Favreau, 1984). The perceived minimum motion of a Gabor stimulus (3.6 deg^2) was measured using a method of adjustment. Isoluminance was calculated as the arithmetic mean of at least 20 settings. Luminance artifacts in the chromatic stimuli were minimized by using low spatial frequencies (0.75–1.5 cpd; Bradley et al., 1992). Since the red–green isoluminant direction was specified within the L/M-cone-contrast plane, it was not orthogonal to the blue–yellow mechanism within the cone-contrast space. Any resulting cross-stimulation of the blue–yellow mechanism would be small, however, and, given the very low cone-contrast sensitivity of the blue–yellow mechanism relative to the red–green (Sankeralli & Mullen, 1996), is highly unlikely to influence the results.

Apparatus and calibrations

Stimuli were displayed on a Sony Trinitron monitor (GDM-F500R) driven by a VSG 2/5 graphics board (Cambridge Research Systems) with 15 bits of contrast resolution, housed in a Pentium PC computer. The frame rate of the display was 76 Hz. The spectral emissions of the red, green, and blue guns of the monitor were calibrated using a PhotoResearch PR-650-PC SpectraScan. The monitor was gamma corrected in software with lookup tables using luminance measurements obtained from an OptiCAL gamma correction system interface with the VSG display calibration software (Cambridge Research Systems). The Smith and Pokorny fundamentals were used for the spectral absorption of the L-, M-, and S-cones. From these data, a linear transform was calculated to specify the phosphor contrasts required for given cone contrasts (Cole & Hine, 1992). The monitor was viewed in a blacked out room. The mean luminance of the display was 60 cd/m^2 . The stimuli were viewed at 60 cm and subtended an area of 254×254 pixels (9×9 degrees). Stimuli were generated online, and a new stimulus was generated for each presentation.

Protocol

In our experiments, cone contrast is expressed in multiples of detection threshold to eliminate the effects of differences in the contrast sensitivity functions of the three post-receptor mechanisms (RG, BY, and Ach) and to allow stimuli to be matched in terms of suprathreshold contrast units (i.e., matched in visibility). For this scaling, contrast detection thresholds were obtained using a 2AFC staircase method for each type of stimulus used: the circular RF patterns, the local parts of an RF4 pattern (corner or side), and the modulated line patterns. A control experiment was also run on some subjects using the same contrast for all stimuli (side, corner, and whole) set to $5 \times$ contrast detection threshold of the whole.

Shape discrimination thresholds were measured using a 2AFC staircase procedure in which the subject was asked to discriminate between a modulated and a non-modulated stimulus (RF or line). Radial amplitude modulation was varied in the case of the RF pattern, and modulation amplitude was varied in the case of the line stimulus. In each trial, one interval contained a non-modulated stimulus and the other contained a modulated stimulus. Subjects were asked to indicate which interval contained the modulated stimulus. In all of our 2AFC staircase procedures, modulation (contrast or shape) was reduced after two correct responses and increased after one wrong response, corresponding to a criterion of 71% correct responses. The change was 50% before the first reversal and 25% after the first reversal. Each session was terminated after 6 reversals, and the detection threshold was computed from the mean of the last five reversals. In the last experiment (Figure 8), thresholds were also measured using a Yes/No staircase procedure in which the subject was asked to indicate if a modulated (RF) pattern or a circle was presented in a single trial. The radial amplitude modulation of the RF pattern was varied as in the 2AFC staircase procedure: shape modulation was reduced after two consecutive responses and increased after one wrong response, resulting in the same response criterion. The other parameters of the staircase remain the same as in the 2AFC procedure.

In all procedures, the exact location of the stimulus was varied randomly from trial to trial about the display center by adding a positional jitter corresponding to 20% of the stimulus radius. The duration of the stimulus presentation interval was 1 s, and the overall contrast of each stimulus was Gaussian enveloped with a sigma of 250 ms centered on the temporal window. Auditory feedback was given after each trial. A black fixation mark was present in the center of the display and subjects were asked to maintain their fixation during the whole presentation. Practice trials were run before the experiments commenced. All experiments were done under binocular conditions.

Observers

The observers were the three authors (KTM, WHB, and IVI) and five additional subjects (ML, WC, LA, MG, and LGS). All have normal or corrected-to-normal vision, and all have normal color vision according to the Farnsworth–Munsell 100 Hue Test.

Results

Dependence of shape discrimination on single stimulus components

In our first experiment, we compare discrimination thresholds for single local components of the stimuli

presented alone to those for the radial frequency patterns as a whole. If the process of global integration is the critical stage at which thresholds for shape perception are determined, we would expect discrimination for the whole shape to be better than for its local components. We used one stimulus cycle of an RF4 pattern centered on the convex (“corner”) or concave (“side”) parts as potentially salient components of the shape, as illustrated in [Figure 1](#) (top) and described by [Equations 5](#) and [6](#) in the [Methods](#) section. Exactly the same experimental protocols were used for the single components and whole RF patterns. The components were presented at the same radius as the whole pattern, and to prevent fixation and examination of the single components, the same fixation mark was used for both types of stimuli (parts and whole) with subjects fixating carefully during stimulus presentation. In addition, the radial phase of the pattern component was varied between stimulus presentations and the absolute position of the pattern center was varied between stimulus presentations (see [Methods](#) section) to avoid anticipation of the component position. For the two highest spatial frequencies (3 and 6 cpd), stimulus phase was varied randomly within 90 degrees (rather than the full 360 degrees) as these thinner contours were harder to localize.

Results are shown in [Figure 1](#) for a spatial frequency of 0.75 cpd, which is low enough to allow both red–green and blue–yellow chromatic stimuli as well as achromatic stimuli to be tested; the data shown are for 5 subjects, with the upper left panel showing the average from all 6 observers tested. Results show that thresholds for the single components are as good as those for the whole RF pattern, and this occurs regardless of whether stimuli are chromatic or achromatic. In [Figure 2](#), we show results for higher spatial frequencies (1.5, 3, and 6 cpd). At 1.5 cpd (top two rows), results for red–green and achromatic stimuli were obtained, but the blue–yellow mechanism cannot be reliably isolated at this spatial frequency. At 3 and 6 cpd (lower two rows), results could only be obtained on achromatic stimuli. As in [Figure 1](#), results in [Figure 2](#) also show that thresholds for the single features are as good as those for the whole RF pattern.

These results show that, over a wide spatial frequency range (0.75–6 cpd) and for chromatic and achromatic stimuli, thresholds for the discrimination of the local components are not significantly different from the discrimination of the RF pattern as a whole. In a control experiment (on subject IVI), we verified that this result does not depend on the contrast scaling of the stimuli (see [Figure 1](#)). Our results indicate that the cues contained within one cycle of the stimulus may limit the overall shape discrimination threshold for the whole stimulus. These results differ from those of previous experiments comparing thresholds for rearranged component parts of an RF pattern and the whole pattern, which found a significant loss of threshold for the discrimination of rearranged RF parts and argued that thresholds for the whole pattern were

limited at a global stage (Hess et al., 1999; Loffler et al., 2003).

Our results on partial contours show similar shape discrimination thresholds for a single stimulus cycle compared to the whole pattern, suggesting that threshold is determined by the information contained within one stimulus cycle. Previous experiments have measured the effect of cycle number on threshold using closed contours and have found a significant increase in threshold as cycle number is increased from a single cycle to the whole pattern (Bell & Badcock, 2008; Hess et al., 1999; Loffler et al., 2003). This effect was greater than that expected on the basis of probability summation, implying threshold discrimination takes advantage of a global pooling mechanism. The discrepancy between our results and previous ones may reveal a genuine difference between using partial versus closed contours. An alternative possibility, however, is that thresholds for discrimination of the partial contour from an arc may be boosted by an extraneous cue not found in the whole RF pattern. We next investigate whether the edges of the partial contour, albeit Gaussian enveloped, provide a shape cue not present in the arc. Such a cue may arise because the contrast modulation is constant along a radial line from the center and thus cuts across the deformed contours at different relative angles, depending on the radial amplitude modulation level and phase of the shape. This potential shape cue may allow the subject to differentiate between segment of a circle and a segment of the modulated contour and enhance discrimination when partial contours are used.

We test for the influence of this potential cue by systematically varying the position (phase) of the Gaussian-enveloped “cut” in the radial frequency pattern for partial contours. The shape cue will be absent when the contour is cut near the peak or trough of the radial modulation as contour modulation is orthogonal to the radial cut at these points (as in the circle), but it will be maximal at the points of inflection (between peak and trough) where the cut is at an angle to the contour. By measuring thresholds as a function of the number of cycles displayed including fractions of a cycle (1/3 to 2), we systematically vary the locations of the cut in the contour and test whether threshold is influenced by a shape cue. In addition, we use two phases for the center of the Gaussian contrast modulation, as in the previous experiment, with the Gaussian centered on either the corners or sides of the pattern, so presenting two opposite phases (positions) of cut location for each cycle number displayed. Results are shown for two observers in [Figures 3A](#) and [3B](#). We find no effect of the phase on the contrast envelope on thresholds and we find no systematic effect for the fraction of cycles displayed between 1 and 2 cycles, indicating that a shape cue generated by the location of the contour cut is not influencing threshold. For fractions of a cycle below 1, thresholds rise significantly indicating that important information has been lost. Interestingly, for these very short contour sections, a

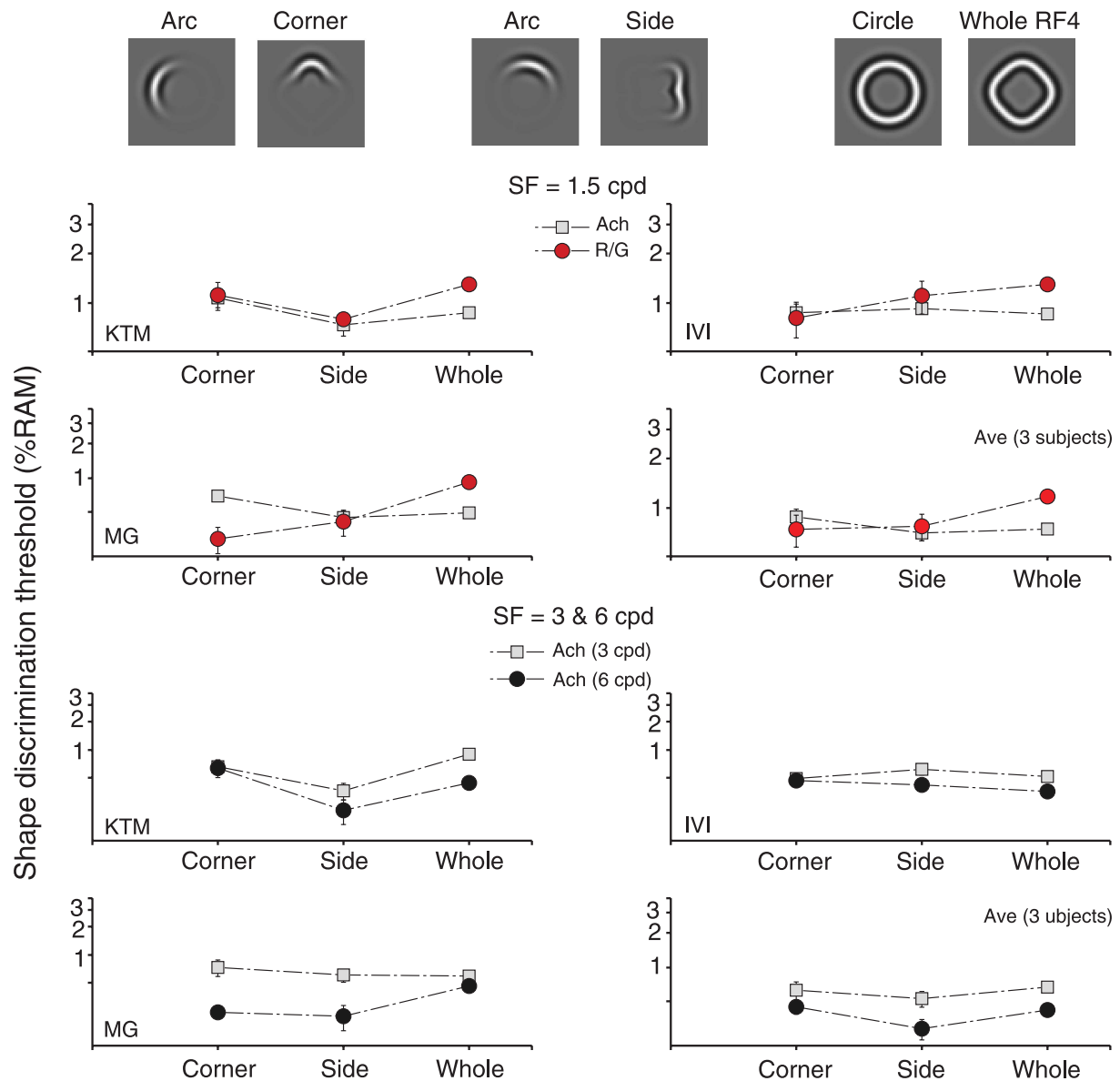


Figure 2. The same format is used as for Figure 1 but with three different spatial frequencies. The four top panels show results for 1.5 cpd (radius = 2.4 degrees) for red–green and achromatic stimuli for three subjects and their average. The lower four panels show results for achromatic stimuli of 3 and 6 cpd as marked for three subjects and their average. Contrasts: for subject KTM and all subjects at 6 cpd, contrast is scaled to 5× contrast detection threshold for each of the test stimuli (corner, side, and whole); for subjects IVI and MG at 1.5 cpd and 3 cpd, the same contrasts are used for each part (5× detection threshold for the whole pattern). Error bars show ±1 SE.

shape cue became visible; contour fractions with the non-orthogonal cut appeared trapezoid compared to the more rectangular circle arc. This cue was only visible below 1 cycle, when thresholds were deteriorating, and so clearly does not account for the low thresholds obtained for 1 cycle and above, where thresholds are stable and no shape cue was visible. We conclude that thresholds for an RF4 are stable from 1 to 4 cycles and are not the result of spurious edge cues.

The data for this experiment also provide a measure of how thresholds depend on the numbers of whole cycles, displayed in partial contours, and allow us to compare the

data with the predicted effect of probability summation on threshold. Shape discrimination thresholds as a function of stimulus cycles displayed (1–4 of an RF4) are plotted in Figures 3C and 3D and compared to a prediction based on probability summation over locally independent detectors (dashed line, see legend for details). Since probability is summed over discrete events (independent detector responses), we included only whole cycles, starting with one cycle. The very sharp decline in thresholds found for contour fractions below 1 cycle (Figures 3A and 3B) supports the use of one cycle as the baseline response over which probability summation may occur. This figure

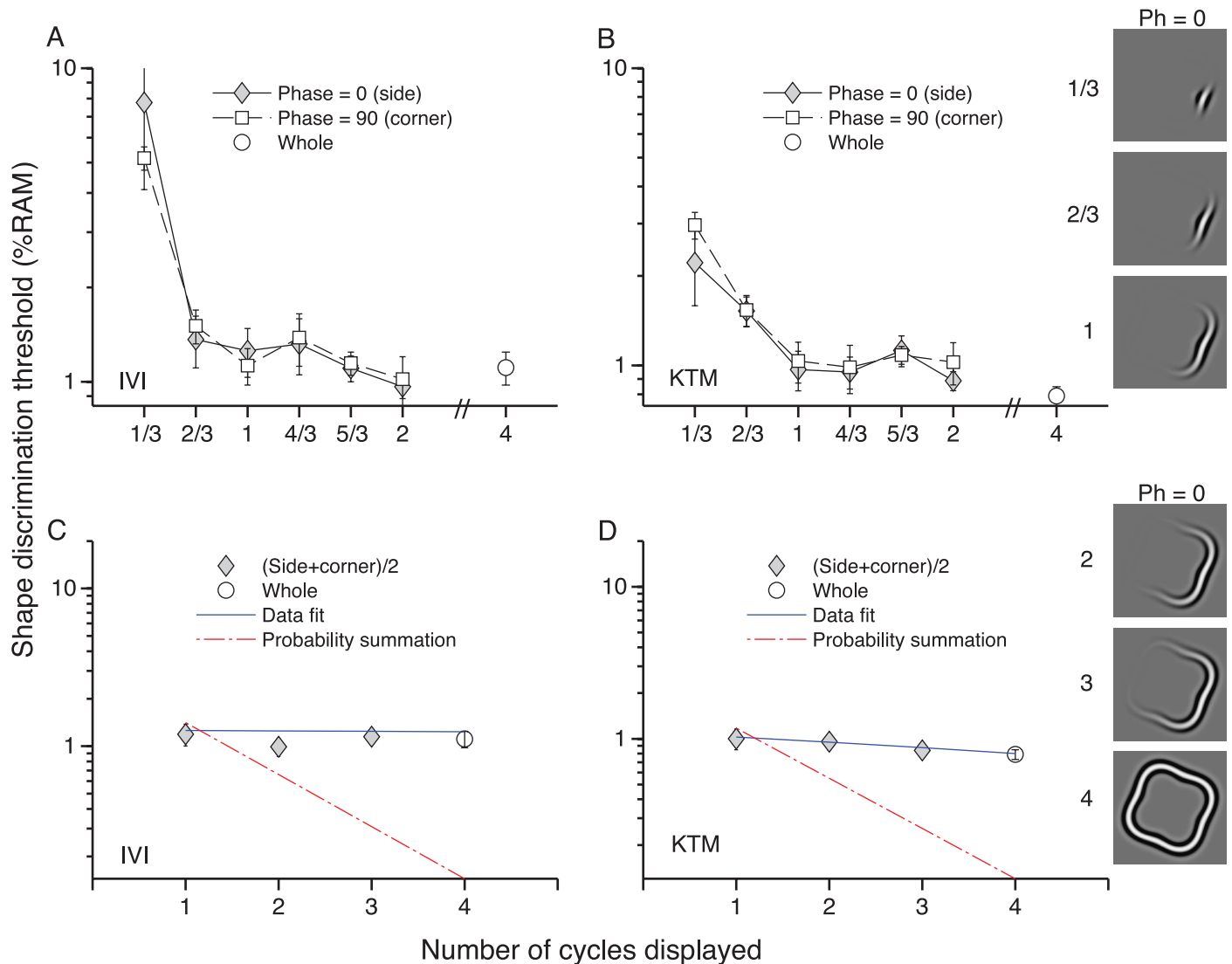


Figure 3. (A, B) Shape discrimination thresholds (% radial amplitude modulation) are plotted as a function of the number of cycles of an RF4 pattern displayed in a partial contour, for two observers. The partial contour was presented in a Gaussian contrast envelope as described in Equation 5, and the Gaussian sigma was systematically varied to display a part of the pattern from 1/3 cycle to 2 cycles. Thresholds for the whole pattern (4 cycles) are included as a reference (hollow circles). The Gaussian envelope was centered on two different phases of the contour: a corner (peak) or a side (inflection), as illustrated in Figures 1 and 2, given by hollow and filled symbols, respectively. Icons illustrating the stimuli for phase = 0 (side) are shown on the right (not exact replications). Values of sigma in degrees for the radial Gaussian contrast envelope used to present each contour part are: 10 (1/3 cycle); 20 (2/3 cycle); 30 (1 cycle); 40 (4/3 cycle); 50 (5/3 cycle); 60 (2 cycles). Error bars show ± 1 SE. (C, D) Data from (A) and (B) are replotted and extended to show shape discrimination thresholds as a function of radial frequency cycles from 1 to 4 (whole). Data points are the average of the two phases tested (side and corner). The solid line shows a linear data fit to the data and the dashed line shows the probability summation prediction, obtained using the method of Loffler et al. (2003, p. 522), with the same exponent value. The function was anchored at 1 stimulus cycle. Error bars show ± 1 SE and are typically less than the symbol size. For KTM, stimulus cone contrast is set to $5\times$ detection threshold for partial stimuli (3.5%, thresholds based on 1 cycle) and whole stimuli (7.7%), respectively. For IVI, the contrast of all stimuli was set to $5\times$ detection threshold for the whole pattern (3%), as in Figure 1.

confirms that the gradual improvement in threshold from 1 to 4 cycles predicted by probability summation is not found in our data. Possible reasons why our data using partial (open) contours and previous data obtained using closed contours may differ are raised in the Discussion section.

A comparison of thresholds for line and radial frequency modulation

In the second experiment, we compare modulation discriminations for the same contour presented either as a line or in the closed form as an RF pattern. We argue that if

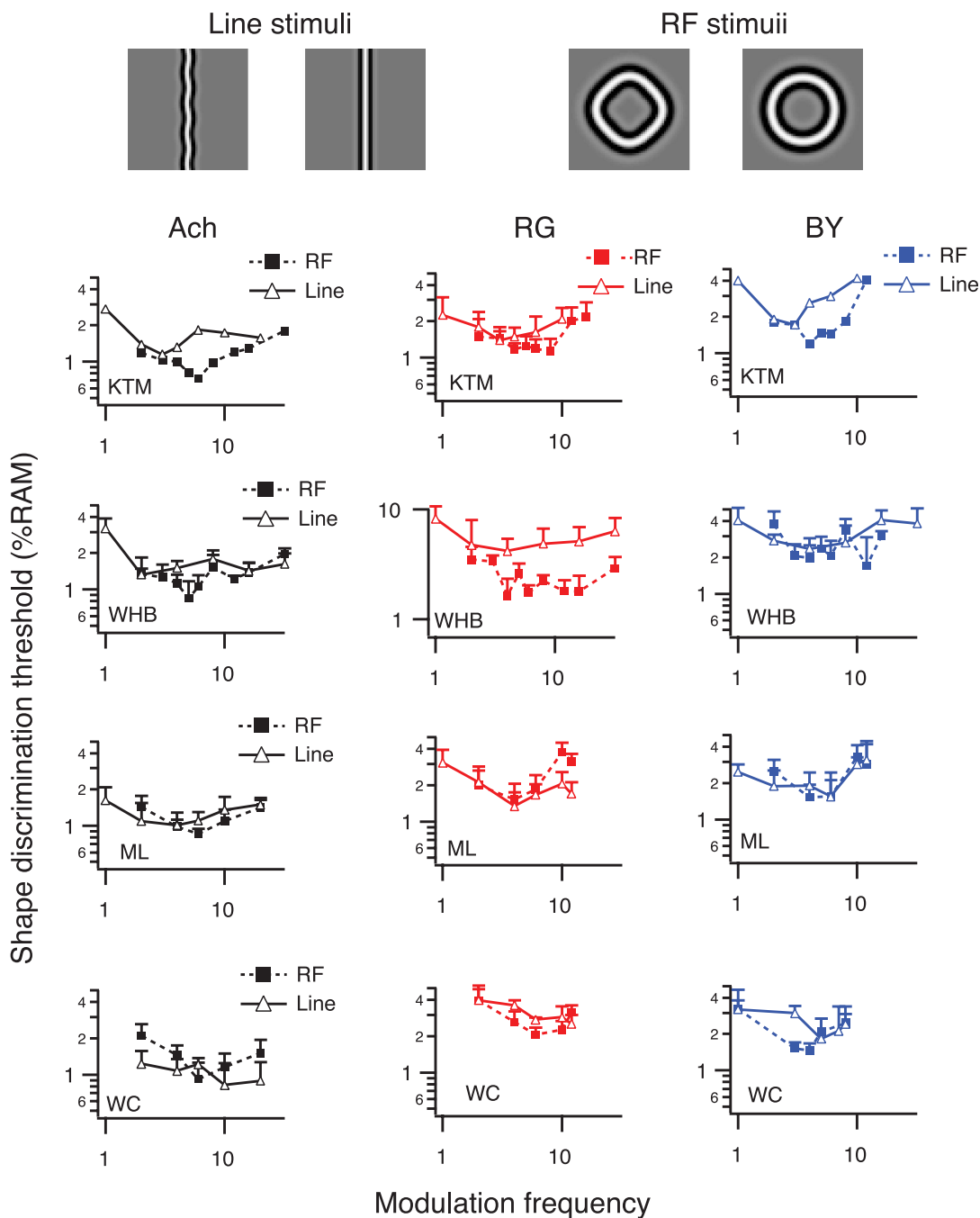


Figure 4. Shape discrimination threshold (% amplitude modulation) is plotted as a function of modulation frequency for modulated line stimuli (hollow triangles), illustrated in the left icon pair, and for radial frequency patterns (filled squares, SF = 0.75 cpd, radius = 2.4 deg), illustrated in the right icon pair. Note that the same contour was used for RF and line stimuli even though it appears of different thicknesses in the icons. Results are given for four subjects (different rows) and for the three conditions (RG, BY, and Ach) in different columns. Error bars show +1 SD.

global processing is limiting the discrimination of the RF patterns, the closed contour that forms a shape should be better discriminated than the linear contour. Results are shown in Figure 4 for the three stimulus conditions (RG, BY, and Ach) for 4 subjects with the line stimulus given by hollow triangles and the circular stimulus by solid squares. A spatial frequency of 0.75 cpd was used to allow both

types of chromatic and achromatic stimuli to be used. Results for the line stimulus, like the RF stimulus, typically show a broad U-shaped function, although somewhat flatter than for the radial stimulus. Previous results using modulated line stimuli with thin line (square-wave) contours have also shown a U-shaped function that, when compared in terms of cycles of modulation per degree of

contour length, are broadly similar to ours (Tyler, 1973). By comparison, thresholds for the RF pattern show a more pronounced U-shape, with a clearer optimum radial frequency around 4 to 6 cycles/circumference and a more marked deterioration in threshold at the higher radial frequencies (Mullen & Beaudot, 2002). Thus, the results do not give a clear answer to the question posed of whether threshold shape discriminations are better for line or RF stimuli; both are similar at low modulation frequencies (2–3 cycles), but radial frequencies typically show an advantage at their peak frequencies of 4–6. Wilkinson et al. (1998) have also pointed out that comparable performances for modulated line and RF stimuli over a range of conditions could indicate the use of local orientation or curvature changes at shape discrimination threshold. They argued against such a similarity experimentally on the grounds that modulation thresholds for RF patterns and lines had a differential dependence on contrast and concluded that the processes underlying the detection of line and radial modulations were different. In the next section, we develop a stimulus-based model in order to explore more fully these differences in threshold and how they may be driven.

A metric for orientation variation in RF and line stimuli at shape discrimination threshold

Our results in Figures 1–3 suggest that the information contained in one RF cycle is sufficient for optimal threshold discrimination and there is no advantage of globally pooling across the whole shape. The question therefore arises as to what the nature of this information might be. As pointed out by Wang and Hess (2005), two distinct local aspects of the RF stimulus potentially distinguish it from the perfect circle: local orientation changes along the contour and local positional changes with respect to the center of the pattern. We calculate the orientation variation contained in one cycle of both the RF and the line stimuli to determine whether these orientation cues are sufficient to support threshold shape discrimination in the RF and line patterns.

An illustration of the local orientation changes in the RF4 pattern is given in Figure 5 with details of the calculations given in Appendix A. In the perfect circle (Figure 5A), the tangent remains at 90 degrees to the radius, whereas in the RF pattern (Figures 5B and 5C) the angle of the tangent varies about 90 degrees (shown in Figure 5D) giving convex and concave regions of the contour, depending on the amplitude of modulation used. This variation in relative orientation is plotted in Figure 5E, based on the formula given in Equation A4 of Appendix A. It can be seen that the local relative orientation varies systematically around the RF contour with only the peaks and troughs of the contour having a tangent of 90 degrees, and the maximum and minimum relative orientations occurring between the peak and trough where the points of inflections are marked. It is

clear from this figure and Equations A4–A9 in Appendix A that the local orientation variation in the patterns depends both on the radial amplitude of modulation (see Figures 5B and 5C) and on the stimulus modulation frequency, with greater local orientation variation for higher radial frequencies.

The question we now address is whether the magnitude of the orientation variation in the radial frequency (RF) stimulus is sufficient to support the shape discrimination thresholds that we measure in the chromatic and achromatic conditions. Appendix A (Equations A1–A9) gives the calculations of the orientation variation around a radially modulated pattern of given amplitude (A) and modulation frequency (ω), expressed as a relative orientation (n , as plotted in Figure 5E). This plot excludes the continuous change in absolute orientation (a) that occurs around a radial contour (shown in Figure 5F). We next calculate a metric for the maximum absolute orientation variation in one cycle of the RF stimulus. First, the orientation change about each contour peak or trough is obtained by differencing the change in absolute orientation of two consecutive inflections. We then calculate the metric for the whole cycle, $\Delta\theta_T$, given by differencing the change in absolute orientation that occurs about a consecutive peak and a trough of the contour cycle. The calculations of $\Delta\theta_T$ and its dependence on radial frequency are given in Equation A9 in Appendix A. We apply this metric to shape discrimination threshold by finding the best fitting value of $\Delta\theta_T$ at our measured shape discrimination thresholds (A). We fit Equation A9 to our data for threshold shape discrimination as a function of radial frequency. This allows us to estimate the difference in orientations about a consecutive peak and a trough of one contour cycle that occurs at the subject's discrimination threshold. We use this as a metric to evaluate the constraints of the orientation cues.

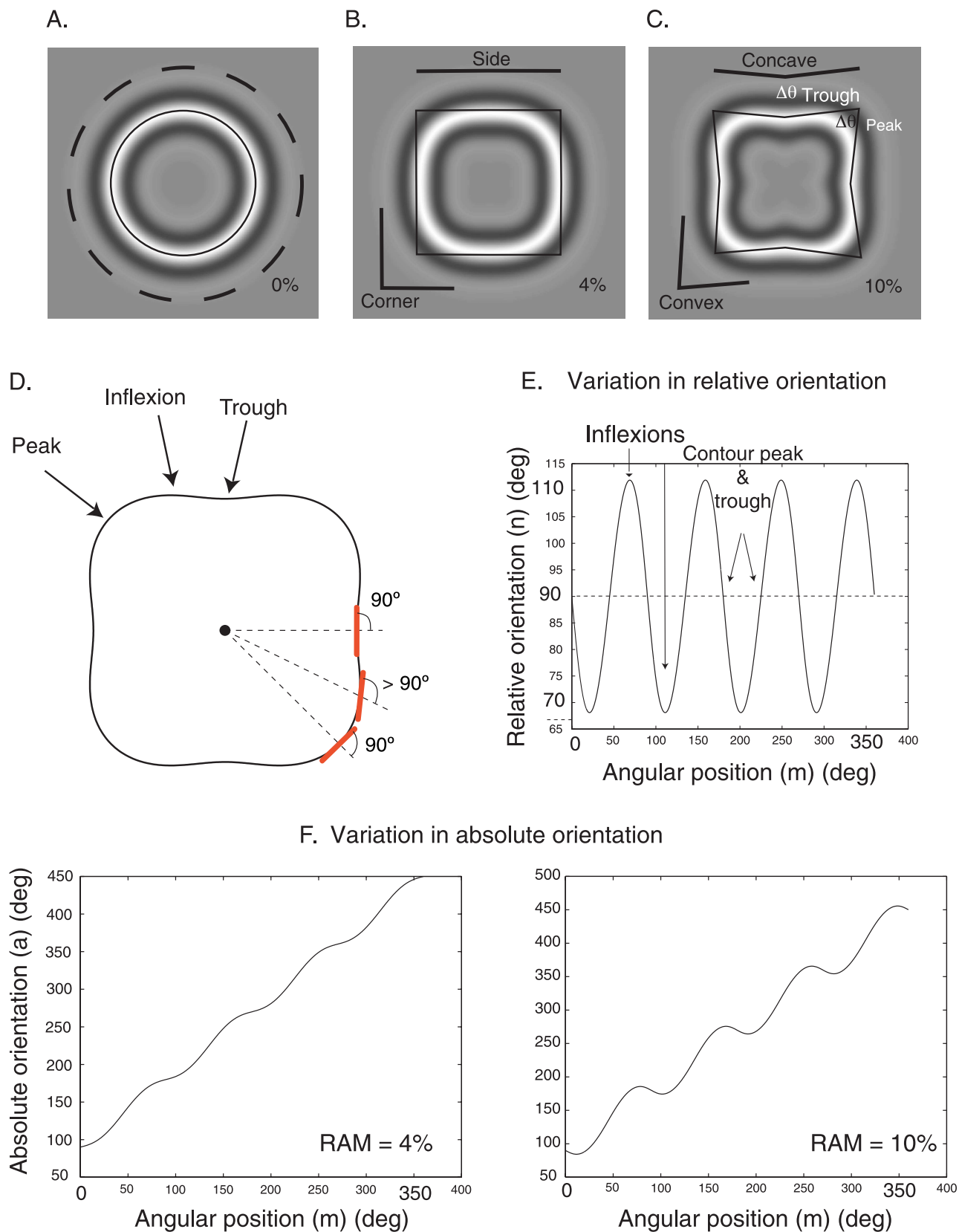
We use a similar approach to calculate the orientation variation in the modulated line stimulus, given in Line pattern section of Appendix A. The maximum variation in orientation along the modulated line (θ_T) is calculated as the difference between the orientations of two consecutive inflection points and is given in Equation A14. The best fitting values of θ_T were obtained by fitting Equation A14 to our data for line modulation thresholds (A) as a function of line modulation frequency. To obtain values for one stimulus cycle, as used for the RF patterns, we report $2 \times (\theta_T)$.

In Figure 6, for two of the four subjects (KTM and WHB), we show the best fitted parameter value for RF stimuli ($\Delta\theta_T$, Equation A9) and for modulated lines ($2\theta_T$, Equation A14). The fitted parameter values and their variances for all four subjects for the achromatic and chromatic stimuli are given in Table 1. Note that there is only one free parameter in the fit. For the RF patterns, data points for radial frequencies in the range of 2–6 cycles/circumference were included in the fit (dashed lines in Figure 6) since thresholds generally decrease within this range. Any non-monotonic, rising thresholds at modulation

frequencies of 5 or 6 were excluded. For the modulated line stimuli, data points for radial frequencies in the range of 1–3 cycles/circumference were included in the fit (solid lines in Figure 6), fewer cycles than for the RF patterns as

the minimum in threshold is less clearly defined (as seen in Figure 4).

These results show three things. First, the initial improvement in shape discrimination thresholds as a function of



radial frequency is broadly consistent with the use of the concomitant increase in stimulus orientation modulation. Second, the stimulus orientation variation in one cycle of the RF pattern at threshold, as determined by the fit, is on average $10 (\pm 2.2)$ degrees for achromatic stimuli and $17.8 (\pm 6.3)$ degrees for chromatic stimuli and, therefore, is well above optimal orientation discrimination thresholds for both chromatic and achromatic stimuli (Beaudot & Mullen, 2005; Heeley, Buchanan-Smith, Cromwell, & Wright, 1997; Webster et al., 1990). Thus, the stimulus orientation variation in one stimulus cycle is a potential and viable cue for shape discrimination threshold. Likewise for line modulations, the average stimulus orientation variation in one cycle at discrimination threshold (6.8 ± 1.1 degrees for achromatic and 13.6 ± 5.2 degrees for chromatic stimuli) is large enough to be used as a cue. We return to these points in the Discussion section. Third, the chromatic stimuli contain greater orientation variation than achromatic stimuli at shape discrimination threshold for both RF and line stimuli. This result is significant at the $p < 0.017$

Figure 5. Calculations of the orientation variation in the RF stimulus. (A–C) Examples of RF stimuli with 0% (perfect circle), 4%, and 10% of radial amplitude modulation. (C) Solid lines connect contour peaks and troughs. The angles $\Delta\theta_{\text{peak}}$ and $\Delta\theta_{\text{trough}}$ represent the difference in absolute orientation between the two consecutive line segments at the peak and trough, respectively. When the radial amplitude modulation (RAM) is low (e.g., 4% in (B)), the troughs (concavities) become secondary peaks (convexities) and the sides appear straighter. (D) A radially modulated contour is drawn as a line with the peaks (“corners”), troughs (“sides”), and points of inflection marked. The short bars show the tangent to the radius (n). The angle of the tangent is 90 degrees only at the peaks and troughs of the contour and the greatest deviation from 90 degrees occurs at the points of inflection. (E) The variation in relative orientation (n) is plotted as a function of angular position (m) around the contour, corresponding to Equation A4. The contour peaks, troughs, and inflection points are marked. The example is for RF = 4 with a radial amplitude modulation of 10%. Note that the most rapid change in orientation occurs at the contour peaks and troughs, between two adjacent points of inflection. The dashed line indicates the angle of the tangent (n) for the perfect circle (90 degrees). For our metric, we calculate the orientation difference at threshold in one stimulus cycle ($\Delta\theta_T$) as the difference between the change in absolute orientation at the peak and the secondary convexity ($|\Delta\theta_{\text{peak}} - \Delta\theta_{\text{trough}}|$), corresponding to twice the full amplitude of the modulation plotted in (E). For a perfect circle, this value ($\Delta\theta_T$) is zero. For completeness, (F) we plot the variation in absolute orientation of the tangent ($a = m + n$) around the contour for the RF stimulus in (B) (RAM = 4%), when there are no concavities, and the stimulus in (C) (RAM = 10%) when peaks and troughs are clearly visible. In our data, the % RAM obtained at shape discrimination threshold is low enough for the stimulus to have no concavities.

level using a Bonferroni-corrected paired t -test (corrected for a 3-way comparison) for the combined data for lines and RF patterns comparing achromatic stimuli with red–green ($p = 0.007$) and blue–yellow ($p = 0.007$). There is no significant difference between values for the red–green and blue–yellow stimuli. This suggests an advantage of achromatic over chromatic stimuli in terms of the utilization of stimulus orientation variation.

Next, we explore the generality of this metric for shape discrimination over a wider range of spatial parameters for the achromatic stimuli. Shape discrimination thresholds for achromatic RF stimuli were measured as a function of radial frequency for a range of contour spatial frequencies (0.75 to 6 cpd) and radii (0.3 to 2.4 degrees). Equation A9 was fitted to the data as before to find the maximum stimulus orientation variation in the stimulus at shape discrimination threshold. Results are shown in Figure 7A. As before, the increase in stimulus orientation variation with modulation frequency is a reasonable predictor of the improvement found in shape discrimination thresholds for radial frequencies from 2 to 6 cycles, with stimulus orientation variation falling between 2.5 and 13 degrees, as marked on the figure. This shows that the stimulus orientation variation is large enough to be discernable over a range of conditions. Stimulus orientation variation also provides a useful metric for the comparison of performance on the task. For both subjects, the most poorly discriminated pattern had the thickest contour (0.75 cpd), and the best discriminated pattern had the thinnest contour (6 cpd). For stimuli of the same spatial frequency (e.g., 6 or 3 cpd), the larger radii were better discriminated than the smaller. To highlight these two effects, we have plotted stimulus orientation modulation as a function of $(\text{SF} * \text{radius})^{-1}$ in Figure 7B. This factor remains constant for stimuli of the same scale: stimuli viewed at different distances in which SF and radius vary in proportion. Results show that these stimuli (SF = 0.75, radius = 2.4 deg; SF = 3.0, radius = 0.6 deg; and SF = 6 cpd, radius = 0.3 deg) group together supporting a size-distance constancy of shape discrimination. In addition, stimuli with the longer radii and/or higher spatial frequency contours are better detected on the basis of lower stimulus orientation modulation than those with the shorter radii and lower spatial frequency contours, with the data showing a monotonic rise between the two. We return to this effect in the Discussion section.

The metric of $\Delta\theta_T$ is based on the intrinsic properties of the RF pattern, because it differences the orientation variation around the peak and trough and predicts that shape discrimination thresholds are invariant whether the RF pattern is compared directly to a perfect circle, as in the 2AFC condition, or it is viewed alone (as in a yes/no procedure). This invariance would support the idea that the local orientation changes used are intrinsic to the contour properties of the RF pattern and as such are robust and useful cues determining the discrimination thresholds.

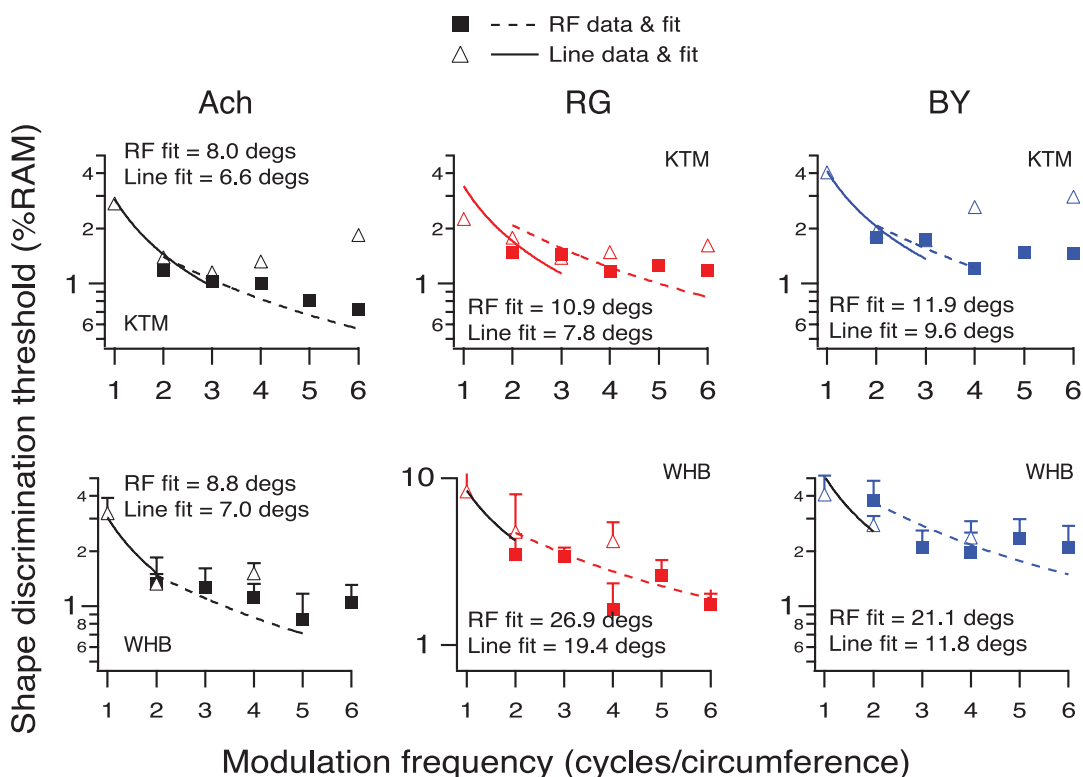


Figure 6. Data points show shape discrimination thresholds for RF (squares, SF = 0.75 cpd, radius = 2.4 deg) and line stimuli (triangles, same contour as for the RF stimuli) as a function of modulation frequency. Dashed lines show the fit of the function describing stimulus orientation variation as a function of radial frequency (Equation A9) to the threshold data, with the fitted value of $\Delta\theta_T$ in degrees marked on the figure. Solid lines show the fit of the function (Equation A14) describing orientation variation as a function of line modulation to the threshold data, with the fitted value of $2\theta_T$ in degrees marked on the figure. Results are shown for 2 of the 4 subjects (KTM and WHB). Note that the fits have one free parameter. Fitted parameter values with standard deviations for all conditions and subjects are shown in Table 1. Chi-squared values of the fits for each subject (KTM, WBH) are: Ach–RF: 0.122, 2.65; Ach–line; 0.815, 0.201; RG–RF: 4.29, 12.81; RG–line: 2.45, 0.0317; BY–RF: 0.835, 10.25; BY–line: 0.299, 1.275. These chi-squared values cannot be assessed statistically using a Q-value since the number of data points (degrees of freedom) is too low. The number of data points cannot be increased since only full cycles are meaningful in the experiment.

Fitted stimulus orientation variation at discrimination threshold

Subject		Ach	RG	BY
KTM	RF	8.0 (0.7)	10.9 (1.1)	11.9 (0.7)
	Line	6.6 (0.3)	7.8 (0.6)	9.4 (1.0)
WHB	RF	8.8 (0.8)	26.9 (2.0)	21.1 (2.5)
	Line	7.0 (0.7)	19.4 (2.6)	11.8 (0.7)
ML	RF	10.4 (0.8)	13.0 (3.5)	15.3 (2.5)
	Line	4.0 (0.5)	8.6 (0.7)	6.0 (0.4)
WC	RF	13.1 (1.9)	26.5 (2.9)	16.6 (1.4)
	Line	9.8 (0.6)	21.6 (0.6)	24.0 (1.6)
Average	RF	10.1 (1.0)	19.3 (2.4)	16.2 (1.8)
	Line	6.8 (0.5)	14.4 (1.1)	12.8 (0.9)

Table 1. Fitted values of stimulus orientation variation calculated for one stimulus cycle at shape discrimination threshold ($\Delta\theta_T$ for RF patterns and $2 \times \theta_T$ for modulated lines) in degrees for each subject and condition. Note: Standard deviations are given in parentheses.

We measured the shape discrimination thresholds as a function of radial frequency with a comparison to a perfect circle, using the standard 2AFC method, and without any direct comparison, using a yes/no method (Figure 8). These results show that there is no significant difference in the performance for these two conditions for achromatic or chromatic stimuli supporting the use of intrinsic contour properties at threshold.

Discussion

Shape processing relies on the gradual transformation of spatial information in hierarchical stages that, through successive integrations, becomes less locally defined and less retinotopically related to the visual input. A threshold

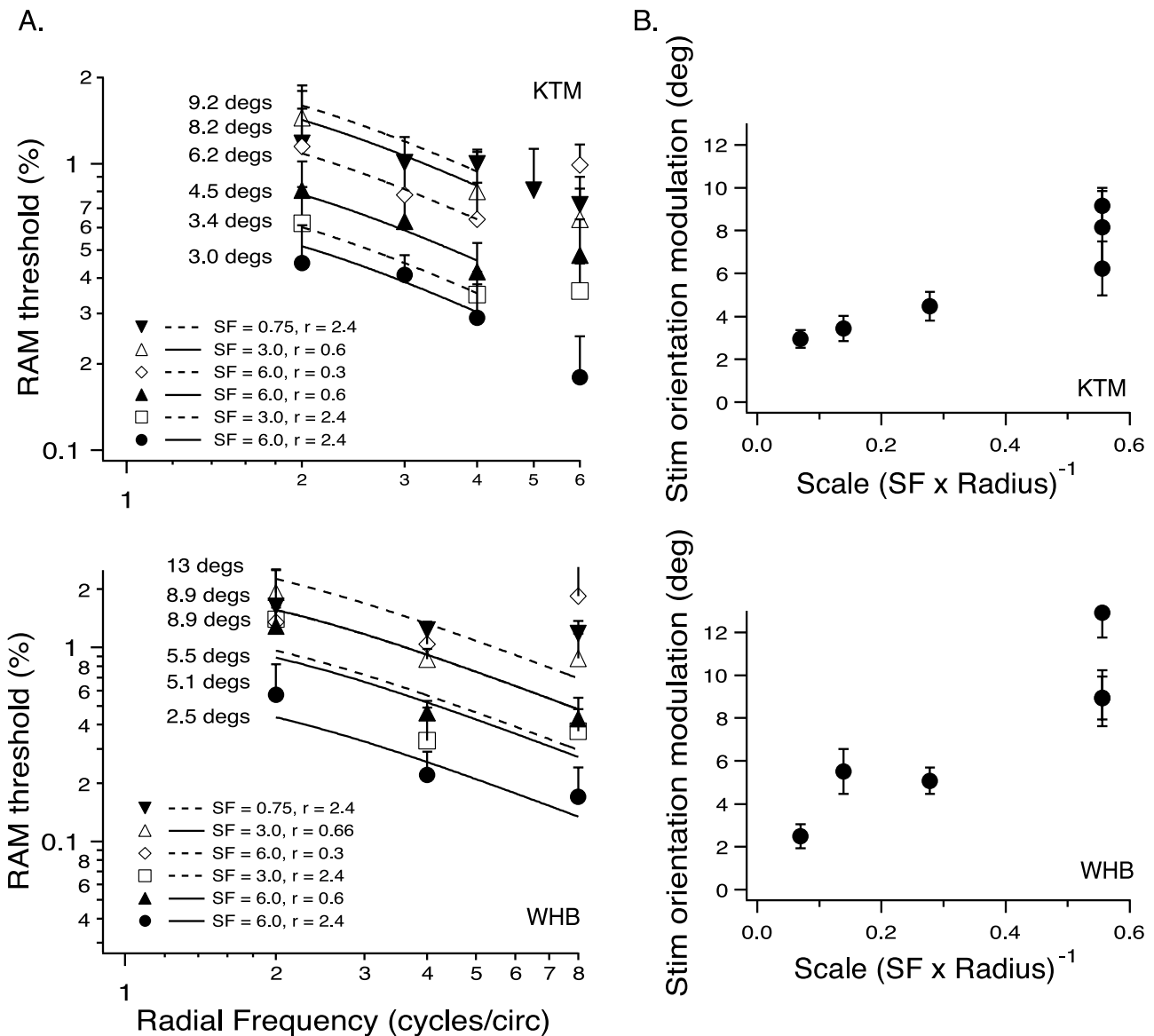


Figure 7. (A) Data points show shape discrimination thresholds (% radial amplitude modulation) plotted as a function of radial frequency for a range of different contour spatial frequencies (SF = 0.75–6 cpd) and radii (0.3–2.4 deg), as indicated by the different symbols in the key. Lines are fits to the data as described in the legend of Figure 6. The fitted value of $\Delta\theta_T$ for each condition is marked beside the fit. Subjects: KTM and WHB. (B) Fitted values of $\Delta\theta_T$ for each condition from (A) are plotted as a function of $(SF * radius)^{-1}$; this value is constant for a stimulus viewed at different distances. Stimuli are achromatic.

for shape discrimination may reveal limitations at any of these sequential stages, from the most local to the most global. The primary aim of our experiments was to assess the relative limitations of the local and intermediate stages of shape processing compared to the global stages, specifically for shape discrimination thresholds for radial frequency stimuli. The crucial distinction we make is that the local and intermediate stages use information contained within one stimulus cycle whereas the global stages require integration or pooling across stimulus cycles to extract the overall shape. A further aim is to understand more precisely

the nature of the information, which limits shape discrimination at threshold.

Evidence that global processing is not limiting RF shape discrimination at threshold

In Figures 1 and 2, we showed that shape discrimination thresholds for a single cycle of the stimulus (centered on the corners or sides) are as good as for the whole radial frequency pattern. This result was consistent across seven

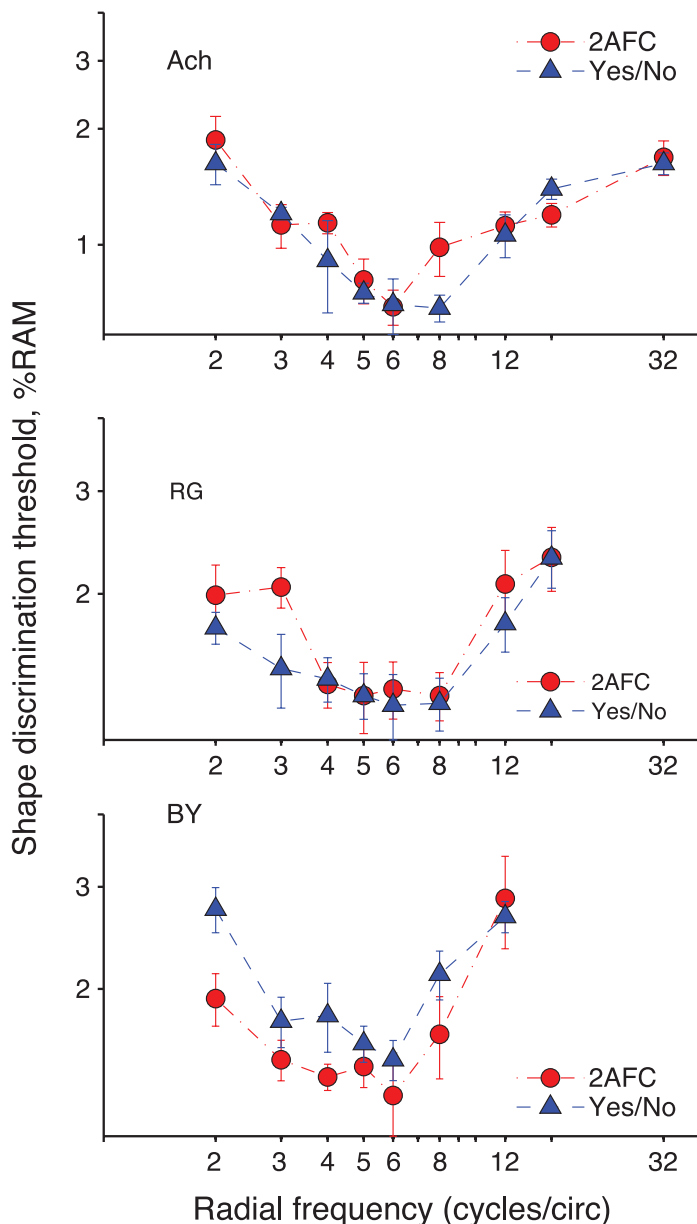


Figure 8. Radial amplitude modulation (%) at shape discrimination threshold is plotted as a function of the radial modulation frequency for RF stimuli (SF = 0.75 cpd, radius = 2.4 deg) that isolate the luminance mechanism (Ach), the L/M-cone opponent (RG) mechanism, and the S-cone opponent (BY) mechanism. Contrasts are scaled to $5\times$ detection threshold. Results are the average of the two subjects tested (KTM and IVI). Shape discrimination thresholds measured without a comparison with the perfect circle (Yes/No procedure) and with a comparison with the perfect circle (2AFC procedure) are compared. Error bars show +1 SE.

different subjects and was robust for both chromatic and achromatic stimuli and across a range of spatial frequencies (0.75–6 cpd). From this, we conclude that there is sufficient information available to support threshold shape discrimination within a single radial frequency cycle.

Hence, it is likely that thresholds are determined at local or intermediate processing stages and not by global mechanisms, which require the pooling of stimulus components across multiple local features. In Figure 3, we show that thresholds are invariant with cycle number from 1 to the complete pattern; however, for stimuli with less than one cycle, thresholds deteriorated sharply. We find no effect of probability summation.

These results and conclusions differ from those of previous studies in which similar hypotheses were tested using different stimulus arrangements. Bell and Badcock (2008), Hess et al. (1999), and Loffler et al. (2003) investigated the effect of cycle number on RF thresholds but using closed contours. In these studies, a single cycle of RF modulation was presented and the two ends of the cycle was closed with a circular contour; the subject had to discriminate between a perfect circle and the circle with an RF cycle embedded in it. Shape discrimination was found to be poorer for single cycles and to improve with increasing cycle number up to the full pattern. Crucially, the improvement with cycle number was greater than expected on the basis of probability summation, implying that discrimination thresholds are enhanced by a process of global pooling across the whole RF pattern. This is very different from the result we obtained using partial (open) contours, in which we find that discrimination thresholds do not depend on the number of cycles presented, and we find no influence of probability summation, arguing strongly against any influence of global pooling. Our control experiments discounted the influence of any shape cues arising from the locations of the contour cuts. Therefore, there appears to be a genuine difference between the effect of cycle number for open and closed contours, in which performance for partial modulations embedded in closed contours is clearly worse than when presented as partial, open contours. There are several potential explanations for why this may be, as discussed below.

Attentional effects may be operating when a single cycle is embedded at random locations within a circular contour, with the hidden target interfering with a search process and reducing performance. There is evidence to support this argument since fixing the phase of the feature improved threshold discrimination, although not up to the levels of the complete RF pattern (Loffler et al., 2003). We therefore suggest that the absence of distracting features, introduced from the presence of a closed contour, may explain why we find thresholds for single cycle in a partial contour to be better than those reported previously for single cycles in closed contours, and as good as for the whole, intact RF pattern. (As an aside, we also note that the effects of pattern cycle number may have been somewhat exaggerated by including fractions of a single cycle (0.5) in the summation calculation (Loffler et al., 2003): our data (Figure 3) show a sudden, steep loss of performance below one cycle (0.33, 0.66). A linear fit of a data set from 0.5 to 4 or 5 cycles, as done by Loffler et al. (2003), tends to exaggerate the slope of the decline compared to that obtained from fitting

only whole cycles from 1 upward.) Our results indicate little or no effect of increasing cycle number. The lack of probability summation in our results is interesting and suggests that other constraints, due to contextual or attentional effects suppressing performance in the whole pattern, may counterbalance any advantage arising from additional cycles.

We also suggest that the results of Hess et al. (1999) demonstrate the influence of attentional effects rather than a disruption of global processing. These authors compared threshold discriminations for an intact RF pattern and a random rearrangement of its parts and found that performance was worse for the rearranged parts. They argued that the rearrangement disrupts global processing, which therefore supports thresholds for the intact RF pattern. Since our results show no loss of performance for a single cycle versus the whole intact pattern, we suggest that some other factor is reducing performance for the multiple rearranged cycles presented by Hess et al. (1999). A strong possibility is that a single feature presented in isolation is easier to attend to than multiple features, since the additional parts act as distracters. We replicated the results of Hess et al. (1999) in 2 subjects for our stimuli (Ach, RG, and BY conditions, subjects WHB and ML) by cutting an RF4 into 4 parts (corresponding to 4 “sides”) and reflecting each part about an axis so that the whole shape was presented as four separate, disconnected pieces. Threshold performance on the stimulus composed of the 4 rearranged parts was, on average, 2.75 times worse than on a single part (i.e., 3.0 for ML and 2.5 for WHB averaged over Ach, RG, and BY conditions), which is compatible with the loss reported by Hess et al. (1999). This suggests that attentional or crowding effects may account for the threshold loss for rearranged multiple pattern parts, rather than a disruption of global processing. Future studies are required to test whether similar contextual effects can account for the apparent difference between closed and open contours.

Another possible effect involves the fact that Loffler et al. (2003) smoothed the transition between the deformation and circular by a D1 applied at the inflection points (zero-crossings). Hess et al. (1999) also cut the contour near an inflection point. These points are where the relative local orientations vary the most (see Figure 4E and Equations A7–A9) and were the stimulus cues we used as metrics in our model. Thus, the poorer performance found for single radial modulations in previous studies (Hess et al., 1999; Loffler et al., 2003) compared to ours might also be due to the missing (smoothed or erased) information at the inflections (zero-crossings). If this were the critical factor in previous studies using closed contours, one would expect a rapid improvement in threshold when changing from one to two cycles of modulation and then a plateau with increasing numbers of cycles. There are no data presented for stimuli with 2 contour cycles in Loffler et al. (2003). There are suggestions of this effect, however, in the data of Hess et al. (1999; Figure 4), although it remains to be tested critically.

An intermediate model of shape processing

There is a clear improvement in shape discrimination threshold with radial frequency for simple shapes up to 6 cycles (our Figure 8, and Mullen & Beaudot, 2002, Figure 4). Here we have argued that this may indicate the use of some aspect of the orientation variation or curvature present in the stimulus contour, since these stimulus cues also increase in magnitude with radial frequency. There is evidence that the corners and sides (Hancock & Peirce, 2008; Poirier & Wilson, 2007), the points of inflection (Wang & Hess, 2005), or all of these (Bell et al., 2010) are important for shape discrimination. The metric we selected is based on the regions of discontinuity in the stimulus contours corresponding to the peaks (“corners”) and troughs (“sides”), where contour orientation changes most rapidly. We use the inflection points to calculate the net change in the orientation around a consecutive peak and trough of the contour in one stimulus cycle. We use a whole cycle since thresholds deteriorate sharply for smaller fractions of a cycle (Figure 3). This model, which requires the analysis of one pattern cycle, is not global since it does not involve the pooling of information across the intact RF shape. On the other hand, it is not local in the sense that it could be computed by single, orientation-tuned neurons in V1. Instead, it requires the estimation of the pattern origin and the appropriate orientation computations at the successive inflection points in a pattern cycle, which is likely to occur at an intermediate stage of contour processing of the type that might be found in V2 or V4 (Pasupathy, 2006; Pasupathy & Connor, 1999).

The use of one stimulus cycle (i.e., the difference in orientation change between the corners and sides) means that the equivalent change in a perfect circle is zero, and the orientation variation metric is effectively intrinsic to the contour. An intrinsic metric implies that RF patterns can be discriminated on the basis of a comparison of the variations in contour orientation within a cycle without recourse to direct comparison with a perfect circle. This is supported by the results of our last experiment (Figure 8), which showed that shape discrimination thresholds obtained without direct comparison with the circle (using a yes/no procedure) were the same as when direct comparison with a circle was made. Wilkinson et al. (1998) have also shown that direct local curvature comparisons with a perfect circle are not required for shape discrimination thresholds, although they argued that this supported a global mechanism.

The importance of the inflection points in shape discrimination might account for why Mullen and Beaudot (2002) found a reduction in performance when contrast modulated contours were used to eliminate either the sides or the corners of an RF4. The contrast attenuation used to obscure sections of the contour displayed only part of each stimulus cycle and eliminated the inflections flanking the corners and the sides. We have also shown here that a performance deficit occurs for fractions of a stimulus cycle. In the

current study, the contrast modulation of the RF contours retained the inflections in the contours and we found that shape discrimination thresholds for local features of the stimulus, corners or sides, were similar and as good as thresholds for whole RF pattern. Mullen and Beaudot (2002) found that sides were more important for shape discrimination than corners, but this may be due to the use of fractions of a stimulus cycle; for such short contour segments, a shape cue may have selectively enhanced discrimination of their stimulus “sides” relative to “corners.”

Fits of Equation A9 (Table 1) give the orientation variation present in one cycle of the stimulus at shape discrimination threshold for radial frequencies of 1–6 cycles. For achromatic stimuli, this is, on average, 10 degrees, and for the two chromatic stimuli, it is 19 (RG) and 16 (BY) degrees. The fact that these values are higher than orientation discrimination thresholds for gratings is not surprising. Sinewave gratings are more narrowly tuned in orientation and support better orientation discrimination than short sections of contour, which are more broadly spread across orientation. Beaudot and Mullen (2005) investigated the relationship between stimulus orientation bandwidth and orientation discrimination for color and achromatic contrast and found that orientation thresholds rise monotonically with bandwidth (from around 1 degree for very narrowband stimuli) to reach thresholds of 8–10 degrees at high stimulus orientation bandwidths (measured for a range of spatial frequencies). Our results indicate that the orientation information in one cycle of the RF stimulus is sufficient to support a threshold shape discrimination task and can predict the threshold improvement for simple shapes as they increase in radial frequency from one (oval-like) to approximately six cycles (hexagon-like).

Effect of color, radius, and spatial frequency on discrimination thresholds

Our results show that chromatic stimuli (shapes and modulated lines) are discriminated using higher orientation variations than are the achromatic ones. The orientation variation at shape discrimination threshold in the RF stimuli is, on average, 1.75 times higher for chromatic compared to achromatic patterns and 2.25 times greater in line stimuli. Previous results using gratings (Webster et al., 1990; Wuerger & Morgan, 1999) or broadband stimuli (Beaudot & Mullen, 2005) at low contrasts have found similar orientation discrimination thresholds for RG and BY stimuli that are approximately 1.5 times greater than that for achromatic stimuli. This result is compatible with the argument that color vision performs less well on the shape discrimination tasks than achromatic vision because it is less sensitive to the orientation variation in the stimuli.

By investigating a range of spatial frequencies and radii for achromatic stimuli (Figure 7), we find that contours are better detected (i.e., on the basis of lower stimulus orien-

tation modulation) for longer radii and/or higher spatial frequencies compared to shorter radii and lower spatial frequencies. This effect may be mediated by two factors: the orientation bandwidth of the stimuli, which depends on the aspect ratio of the local contour, and the deterioration in orientation discrimination that occurs at low spatial frequencies (Burr & Wijesundra, 1991), which may account for the loss at the lower spatial frequencies.

We also find that lines are discriminated on the basis of moderately lower orientation variations than the RF patterns. Unlike the RF pattern, the line passes through the fovea, which may aid in its discrimination. Although not conclusive, the line results are compatible with the conclusion that there is no threshold advantage in pooling across cycles in the RF pattern, arguing against global pooling at threshold.

While our results suggest that the improvement in discrimination thresholds for RF patterns as a function of shape frequency can potentially be explained by the increase in orientation variation within each stimulus cycle, rather than by summation across the global shape, the question of what limits discrimination at higher radial frequencies remains open. We find that thresholds deteriorate above a radial frequency of around 6 cycles, forming a U-shaped function for the spatial frequency range measured (0.75 to 6 cpd). Bell et al. (2007) proposed that shape discrimination gives way to the discrimination of edge effects as radial frequency increases. Mullen and Beaudot (2002) have shown that this high radial frequency loss depends on the aspect ratio of the contour, namely its thickness (peak spatial frequency) compared to the radial cycle length, with an elevation in threshold occurring when the radial cycle length is reduced below approximately two contour widths. This suggests that the factor limiting radial modulation thresholds at high radial frequencies is geometric in nature and may be related to the aspect ratio of the visual neurons underlying this edge discrimination in the visual system. This has not been tested for very thin contours (e.g., 8–16 cpd) of the type used by Wilkinson et al. (1998) since these patterns would need higher RFs than were used to reach the stimulus aspect ratio thought to be threshold limiting.

Concluding comment

Psychophysical thresholds by their nature reveal the most sensitive stage of a visual process. Once RF stimuli become suprathreshold, all stages of the shape processing hierarchy are active. We have presented evidence suggesting that simple, shape discrimination thresholds are not limited by global processes, which require pooling of information around the whole shape. This does not, however, exclude the contribution of global processes to the perception of suprathreshold, well-defined RF patterns. We suggest that for the very low modulation amplitudes obtained at shape

discrimination threshold, non-global, orientation variations may be the only or the most effective cue available. For well-defined shapes with suprathreshold level of modulation, such as those used in adaptation (Bell, Dickinson, & Badcock, 2008; Bell et al., 2009; Bell & Kingdom, 2009; Hancock & Peirce, 2008) and fMRI experiments (Dumoulin & Hess, 2007; Wilkinson et al., 2000), all stages of shape processing will be enabled and such approaches may prove more successful at separating the differential contributions of the lower and the higher stages of the processing hierarchy.

Appendix A

In this appendix, we derive a model that predicts amplitude modulation thresholds as function of the modulation frequency based on the perception of the orientation changes along: (i) a radially modulated circular pattern and (ii) a line pattern.

Circular pattern

Given a curve as illustrated in Figure A1 and some origin O , the orientation a of the tangent to the curve at a point P is given by

$$a = m + n, \quad (\text{A1})$$

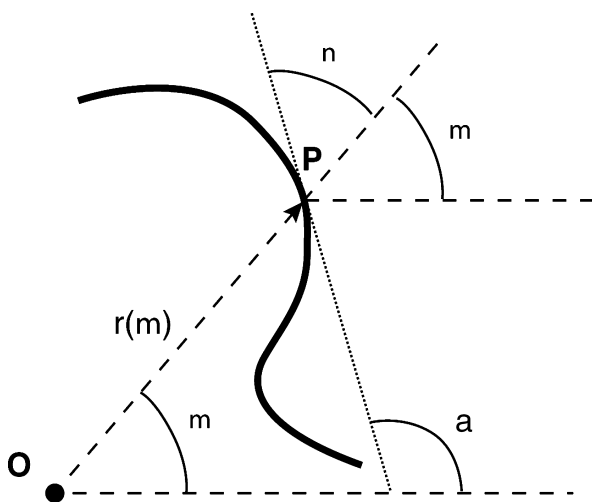


Figure A1. The thick curve represents the radial modulation of the pattern, O represents the origin, P represents any given point on the curve, the dotted line represents the tangent to the curve in P , m represents the absolute angle (or orientation) of the line OP , $r(m)$ represents the distance between O and P , n represents the angle between the line OP and the tangent of the curve in P , and a represents the absolute angle of the tangent in P .

where n is the angle between the axis OP and the tangent to the curve, and m is the angular position at point P .

The direction of the curve in polar coordinates relatively to the axis OP is given by

$$\tan(n) = r/r', \quad (\text{A2})$$

where r and r' denote the radius and its derivative at point P .

A RF pattern is characterized by a radial modulation given by

$$r(m) = R_0[1 + A \cdot \sin(\omega \cdot m + \varphi)], \quad (\text{A3})$$

where m is the angular position, R_0 is the mean radius, A is the amplitude modulation, ω is the radial frequency, and φ is the angular phase.

Solving for n in Equation A2 with r given by Equation A3 leads to

$$n = \arctan \left[\frac{1 + A \cdot \sin(m \cdot \omega + \varphi)}{A \cdot \omega \cdot \cos(m \cdot \omega + \varphi)} \right]. \quad (\text{A4})$$

For an unmodulated pattern (i.e., circular, $A = 0$), n is constant ($\pi/2$) and there is no change in relative orientation around the pattern. For a modulated pattern, n oscillates around $\pi/2$ (at the peaks and troughs of the radial modulation) between maximum and minimum relative orientations given by $\partial n / \partial m = 0$:

$$m_{\min} = -\frac{\varphi + \arcsin(A)}{\omega} + k \frac{2\pi}{\omega}, \quad k \in \mathbb{Z}, \quad (\text{A5.1})$$

and

$$m_{\max} = \frac{\pi}{\omega} + \frac{\varphi + \arcsin(A)}{\omega} + k \frac{2\pi}{\omega}, \quad k \in \mathbb{Z}. \quad (\text{A5.2})$$

These angular positions correspond to the inflection points between the peaks and troughs, and their respective absolute orientations provide estimates of the orientation of the edges (we simplified the expressions by setting $\varphi = 0$):

$$n(m_{\max}) = -\arctan \left(\frac{\sqrt{1-A^2}}{A\omega} \right), \quad (\text{A6.1})$$

and

$$n(m_{\min}) = \arctan \left(\frac{\sqrt{1-A^2}}{A\omega} \right). \quad (\text{A6.2})$$

Their absolute orientation is then given by $a(m_i) = m_i + n(m_i)$.

The maximum changes in absolute orientation appear at the peaks and troughs of the RF patterns, and they can be measured by the difference between the absolute orientations of 2 consecutive inflection points given by

$$\Delta\theta = \frac{\pi + 2\arcsin(A)}{\omega} - 2\arctan\left(\frac{\sqrt{1-A^2}}{A\omega}\right). \quad (\text{A7})$$

At detection thresholds ($A \ll 1$), the orientation difference at the peaks and troughs is approximately given by

$$\Delta\theta_{\text{peak}} \approx \frac{\pi}{\omega} + 2A \cdot \frac{\omega^2 + 1}{\omega}, \quad (\text{A8.1})$$

and

$$\Delta\theta_{\text{trough}} \approx \frac{\pi}{\omega} - 2A \cdot \frac{\omega^2 + 1}{\omega}. \quad (\text{A8.2})$$

This model can account for the decrease of the RAM with radial frequencies. The larger orientation changes along a RF pattern occur at specific points, the corners and troughs. The changes of orientation at the peaks and troughs are given by Equations A8.1 and A8.2. Note that $\Delta\theta_{\text{peak}}$ is always positive, and that the sign of $\Delta\theta_{\text{trough}}$ changes at $A = \frac{\pi}{2(\omega^2+1)}$, that is $\Delta\theta_{\text{trough}}$ is positive when $A < \frac{\pi}{2(\omega^2+1)}$ and is negative when $A > \frac{\pi}{2(\omega^2+1)}$. This indicates that for high values of A , the RF patterns are composed of peaks and troughs alternating around its circumference, and for small enough values of A , they are composed of peaks only (Figures 5B, 5C, 5F, and 5G). A RF pattern is discernible from a circular or non-modulated pattern when the difference between $\Delta\theta_{\text{peak}}$ and $\Delta\theta_{\text{trough}}$ (both positive, i.e., convex) is above a discrimination threshold:

$$\Delta\theta_{\text{peak}} - |\Delta\theta_{\text{trough}}| > \Delta\theta_{\text{T}}, \text{ that is } A > \frac{\omega \cdot \Delta\theta_{\text{T}}}{4(\omega^2 + 1)}. \quad (\text{A9})$$

We use Equation (A9) to fit the experimental data.

Line pattern

A linear pattern is characterized by a linear modulation given by

$$\begin{aligned} y &= R_o \cdot A \cdot \sin(\omega \cdot m + \varphi) \\ x &= R_o \cdot (m + \pi), \end{aligned} \quad (\text{A10})$$

where m varies between $-\pi$ and $+\pi$ to ensure that the linear pattern has the same length than a circular pattern with mean radius R_o , A is the amplitude modulation

($A = \Delta R/R$), ω is the modulation frequency, and φ is the modulation phase (for simplicity, $\varphi = 0$).

The absolute orientation α along this curve is directly related to the slope:

$$\alpha = \arctan\left(\frac{\partial y}{\partial x}\right). \quad (\text{A11})$$

The inflection points between the peaks and troughs along the line pattern are given by

$$m_1 = k \cdot \frac{2\pi}{\omega}, \quad k \in \mathbb{Z}, \quad (\text{A12.1})$$

and

$$m_2 = \frac{\pi}{\omega} + k \cdot \frac{2\pi}{\omega}, \quad k \in \mathbb{Z}. \quad (\text{A12.2})$$

The maximum changes in absolute orientation appear at the peaks and troughs of the line patterns, and they can be measured by the difference between the absolute orientations of 2 consecutive inflection points (m_1 and m_2) given by

$$\Delta\theta = \pm 2\arctan(A\omega). \quad (\text{A13})$$

Note that contrarily to the circular pattern, the orientation difference is the same at peaks and troughs. This difference is perceived when it reaches a given threshold, $|\Delta\theta| > \theta_{\text{T}}$, that is for

$$A > \frac{1}{\omega} \cdot \tan\left(\frac{\theta_{\text{T}}}{2}\right). \quad (\text{A14})$$

We use this equation to fit the experimental data obtained for the line patterns.

Acknowledgments

This study was funded by a CIHR Grant to K. T. Mullen (MOP-10819). The authors thank Michael Lo, William Chu, Liza Azef, Luis Garcia Suarez, and Mina Gheiratmand for their help in collecting data. We thank the two anonymous reviewers and the handling editor (James Elder) for insightful comments.

Commercial relationships: none.

Corresponding author: Kathy T. Mullen.

Email: kathy.mullen@mcgill.ca.

Address: McGill Vision Research, Department of Ophthalmology H4.14, McGill University, 687 Pine Ave West, Montreal, Quebec, Canada H3A 1A1.

References

- Beaudot, W. H., & Mullen, K. T. (2005). Orientation selectivity in luminance and color vision assessed using 2-d band-pass filtered spatial noise. *Vision Research*, *45*, 687–696.
- Bell, J., & Badcock, D. R. (2008). Luminance and contrast cues are integrated in global shape detection with contours. *Vision Research*, *48*, 2336–2344.
- Bell, J., Badcock, D. R., Wilson, H., & Wilkinson, F. (2007). Detection of shape in radial frequency contours: Independence of local and global form information. *Vision Research*, *47*, 1518–1522.
- Bell, J., Dickinson, J. E., & Badcock, D. R. (2008). Radial frequency adaptation suggests polar-based coding of local shape cues. *Vision Research*, *48*, 2293–2301.
- Bell, J., Gheorghiu, E., & Kingdom, F. A. (2009). Orientation tuning of curvature adaptation reveals both curvature-polarity-selective and non-selective mechanisms. *Journal of Vision*, *9*(12):3, 1–11, <http://www.journalofvision.org/content/9/12/3>, doi:10.1167/9.12.3. [PubMed] [Article]
- Bell, J., & Kingdom, F. A. (2009). Global contour shapes are coded differently from their local components. *Vision Research*, *49*, 1702–1710.
- Bell, J., Hancock, S., Kingdom, F. A., & Peirce, J. W. (2010). Global shape processing: Which parts form the whole? *Journal of Vision*, *10*(6):16, 1–13, <http://www.journalofvision.org/content/10/6/16>, doi:10.1167/10.6.16. [PubMed] [Article]
- Bradley, A., Zang, L., & Thibos, L. N. (1992). Failures of isoluminance caused by ocular chromatic aberration. *Applied Optics*, *31*, 3657–3667.
- Burr, D. C., & Wijesundra, S. A. (1991). Orientation discrimination depends on spatial frequency. *Vision Research*, *31*, 1449–1452.
- Cavanagh, P., Tyler, C. W., & Favreau, O. E. (1984). Perceived velocity of moving chromatic gratings. *Journal of the Optical Society of America A*, *1*, 893–899.
- Cole, G. R., & Hine, T. (1992). Computation of cone contrasts for color vision research. *Behavior Research Methods, Instruments, & Computers*, *24*, 22–27.
- Cole, G. R., Hine, T., & McIlhagga, W. (1993). Detection mechanisms in L-, M-, and S-cone contrast space. *Journal of the Optical Society of America A*, *10*, 38–51.
- Dobbins, A., Zucker, S. W., & Cynader, M. S. (1987). Endstopped neurons in the visual cortex as a substrate for calculating curvature. *Nature*, *329*, 438–441.
- Dobbins, A., Zucker, S. W., & Cynader, M. S. (1989). Endstopping and curvature. *Vision Research*, *29*, 1371–1387.
- Dumoulin, S. O., & Hess, R. F. (2007). Cortical specialization for concentric shape processing. *Vision Research*, *47*, 1608–1613.
- Eskew, R. T., McLellan, J. S., & Giulianini, F. (1999). Chromatic detection and discrimination. In K. R. Gegenfurtner & L. T. Sharpe (Eds.), *Color vision: From molecular genetics to perception* (pp. 345–368). Cambridge, UK: Cambridge University Press.
- Gallant, J. L., Braun, J., & Van Essen, D. C. (1993). Selectivity for polar, hyperbolic, and Cartesian gratings in macaque visual cortex. *Science*, *259*, 100–103.
- Gallant, J. L., Shoup, R. E., & Mazer, J. A. (2000). A human extrastriate area functionally homologous to macaque V4. *Neuron*, *27*, 227–235.
- Hancock, S., & Peirce, J. W. (2008). Selective mechanisms for simple contours revealed by compound adaptation. *Journal of Vision*, *8*(7):11, 1–10, <http://www.journalofvision.org/content/8/7/11>, doi:10.1167/8.7.11. [PubMed] [Article]
- Heeley, D. W., Buchanan-Smith, H. M., Cromwell, J. A., & Wright, J. S. (1997). The oblique effect in orientation acuity. *Vision Research*, *37*, 235–242.
- Hess, R. F., Wang, Y.-Z., & Dakin, S. C. (1999). Are judgements of circularity local or global? *Vision Research*, *39*, 4354–4360.
- Hubel, D. H., & Wiesel, T. N. (1968). Receptive fields and functional architecture of monkey striate cortex. *The Journal of Physiology*, *195*, 215–243.
- Jeffrey, B. G., Wang, Y. Z., & Birch, E. E. (2002). Circular contour frequency in shape discrimination. *Vision Research*, *42*, 2773–2779.
- Levi, D. M., & Klein, S. A. (2000). Seeing circles: What limits shape perception? *Vision Research*, *40*, 2329–2339.
- Loffler, G. (2008). Perception of contours and shapes: Low and intermediate stage mechanisms. *Vision Research*, *48*, 2106–2127.
- Loffler, G., Wilson, H. R., & Wilkinson, F. (2003). Local and global contributions to shape discrimination. *Vision Research*, *43*, 519–530.
- Mullen, K. T., & Beaudot, W. H. (2002). Comparison of color and luminance vision on a global shape discrimination task. *Vision Research*, *42*, 565–575.
- Pasupathy, A. (2006). Neural basis of shape representation in the primate brain. *Progressive Brain Research*, *154*, 293–313.
- Pasupathy, A., & Connor, C. E. (1999). Responses to contour features in macaque area V4. *Journal of Neurophysiology*, *82*, 2490–2502.
- Poirier, F. J., & Wilson, H. R. (2007). Object perception and masking: Contributions of sides and convexities. *Vision Research*, *47*, 3001–3011.

- Sankeralli, M. J., & Mullen, K. T. (1996). Estimation of the L-, M- and S-cone weights of the post-receptoral detection mechanisms. *Journal of the Optical Society of America A*, *13*, 906–915.
- Sankeralli, M. J., & Mullen, K. T. (1997). Postreceptoral chromatic detection mechanisms revealed by noise masking in three-dimensional cone contrast space. *Journal of the Optical Society of America A*, *14*, 2633–2646.
- Smith, V. C., & Pokorny, J. (1975). Spectral sensitivity of the foveal cone photopigments between 400 and 500 nm. *Vision Research*, *15*, 161–171.
- Tyler, C. W. (1973). Periodic vernier acuity. *The Journal of Physiology*, *228*, 637–647.
- Wang, Y. Z., & Hess, R. F. (2005). Contributions of local orientation and position features to shape integration. *Vision Research*, *45*, 1375–1383.
- Webb, B. S., Roach, N. W., & Peirce, J. W. (2008). Masking exposes multiple global form mechanisms. *Journal of Vision*, *8*(9):16, 1–10, <http://www.journalofvision.org/content/8/9/16>, doi:10.1167/8.9.16. [PubMed] [Article]
- Webster, M. A., De Valois, K. K., & Switkes, E. (1990). Orientation and spatial-frequency discrimination for luminance and chromatic gratings. *Journal of the Optical Society of America A*, *7*, 1034–1049.
- Wilkinson, F., James, T. W., Wilson, H. R., Gati, J. S., Menon, R. S., & Goodale, M. A. (2000). An fMRI study of the selective activation of human extrastriate form vision areas by radial and concentric gratings. *Current Biology*, *10*, 1455–1458.
- Wilkinson, F., Wilson, H. R., & Habak, C. (1998). Detection and recognition of radial frequency patterns. *Vision Research*, *38*, 3555–3568.
- Wilson, H. R. (1999). Non-Fourier cortical processing in texture, form, and motion. In P. S. U. E. G. Jones (Ed.), *Cerebral cortex: Models of cortical circuitry* (vol. 13, pp. 445–477). New York: Kluwer Academic/Plenum Publishers.
- Wilson, H. R., & Wilkinson, F. (1997). Evolving concepts of spatial channels in vision: From independence to nonlinear interactions. *Perception*, *26*, 939–960.
- Wuerger, S. M., & Morgan, M. J. (1999). Input of long- and middle-wavelength-sensitive cones to orientation discrimination. *Journal of the Optical Society of America A*, *16*, 436–442.